

# Optimization design and reality of the virtual cutting process for the boring bar based on PSO-BP neural networks

Yu-shan Sun<sup>1</sup> · Qiang Zhang<sup>2</sup>

Received: 1 December 2016 / Accepted: 13 February 2017 / Published online: 1 March 2017  
© The Natural Computing Applications Forum 2017

**Abstract** Based on the traditional boring bar, a boring bar with friction damper is proposed in the paper. Firstly, the frequency response under different pressures is computed primarily based on the theory, which shows that the proposed boring bar has a certain vibration reduction effect. Secondly, the finite element model of the boring bar is built, and the first 6-order modes are computed, whose results are compared with the experimental value. As a result, the virtual reality of the boring bar is achieved. They are consistent with each other, which show that the finite element model is reliable. Then, the experimental cutting process of the boring bar is researched, which is compared with the simulation model with good coincidence. It is found from the result that the cutting simulation model of the boring bar is effective. Later, based on the verified simulation model, the positive pressure between the friction vibrator and boring bar, cutting speed, feed rate, back cutting depth and other parameters are changed to study the vibration reduction effects of the boring bar with friction damper. PSO (particle swarm optimization)-BP (back-propagation) neural network is then used to optimize the cutting process of the boring bar, and the optimal cutting parameters can be obtained. Finally, these optimized parameters are applied in the boring bar, the vibration reduction effect of the boring bar is verified by means of experiments, and the corresponding result shows that the proposed optimization in this paper is feasible. We can

obtain higher quality work piece when we use this boring bar in the actual engineering.

**Keywords** Boring bar · Virtual reality · PSO-BP neural network · Vibration reduction · Optimization design

## 1 Introduction

With the constant development of mechanical manufacturing technology, increasingly high precisions have been required on cutting technology in actual engineering, especially some industries demanding high precisions. When the boring bar has a large overhanging, produced work pieces cannot meet design requirements as vibration cannot be excited by static stiffness or dynamic stiffness. The machining characteristics of the boring bar have a poor static stiffness and dynamic stiffness. In high-speed cutting process, even slight vibration will lead to the instability of high-speed machining process and the serious damage of cutting tools due to the high rotation speed of machine tool spindle. Therefore, studying how to reduce vibration is necessary to lower machining costs and improve the high-speed machining efficiency of grinding tools [1–4]. To reduce the vibration amplitude of the boring bar head, the following several measures are mainly taken: (1) Conduct optimization design for the boring bar head and reduce the weight of the boring bar head on the premise of ensuring the high stiffness of the boring bar; (2) Adopt composite materials to produce the boring bar, improve the static stiffness and dynamic stiffness of the boring bar and increase the damping ratio of the boring bar; (3) Take advantage of the hollow structure of the boring bar and subtly design damper to consume vibration energy and improve the dynamic performance of the boring bar.

✉ Yu-shan Sun  
sunyushan@hrbeu.edu.cn; sunyushan2009a@163.com

<sup>1</sup> Science and Technology on Underwater Vehicle Laboratory, Harbin Engineering University, Harbin 150001, China

<sup>2</sup> Technology Research and Development Center, Harbin No. 1 Tool Manufacture Corporation Ltd., Harbin 150078, China

To solve the vibration problem of the boring bar and improve the machining precision of cutting of the boring bar, currently, a large number of scholars have made many attempts and conducted numerous studies. Sandvik in Sweden produced boring bars with damping vibration attenuation whose principle added a damping system to the section where the boring bar was close to the tool, improving the dynamic performance of the boring bar [5]. Japanese Mitsubishi Corporation and Toshiba Corporation produced series damping boring bars whose design thought was to optimize the boring bar head, adopt unique section and try to reduce the weight of its head on the premise of ensuring the strength of the boring bar [6]. Zhai et al. [7] also designed a kind of high-frequency, precise and servo boring bars from a dynamic perspective and experimentally verified the superiority of the structure. Mei et al. [8] proposed an innovative chatter suppression method based on a magnetorheological (MR) fluid-controlled boring bar. The MR fluid, which can change stiffness consecutively by varying the strength of the applied magnetic field, was applied to adjust the stiffness of the boring bar and suppress chatter. An approach to study the whirling motion of the deep hole boring system is presented by introducing the system excitation in the form of internal forces between the boring bar and the work piece, and external suppression forces will reduce the whirl amplitude at the same locations. The researched result was also verified by the corresponding experiment [9].

The mentioned studies mainly improve the internal structure of the boring bar and need relatively high design cycle and cost. Aiming at this problem, this paper firstly adopts finite element method to improve various parameters in the cutting process of the boring bar and study the impact of cutting parameters on the precision of the boring bar. As a result, the virtual reality of the boring bar is achieved. Then, this paper uses Elman BP neural network to optimize the cutting process of the boring bar and get the optimal cutting parameters so as to obtain the result of high cutting precision on the prerequisite of maintaining the original structure of the boring bar.

## 2 Theoretical model of the boring bar

Based on the friction damper principle, boring bar is designed. There is friction vibrator, and permanent magnet poles are in front cavity of the boring bar to reduce vibration.

### 2.1 Mechanical model in sliding friction state

Kinetic model of the boring bar in sliding friction state is shown in Fig. 1. Figure 1 is from the professional drawing software AutoCAD.

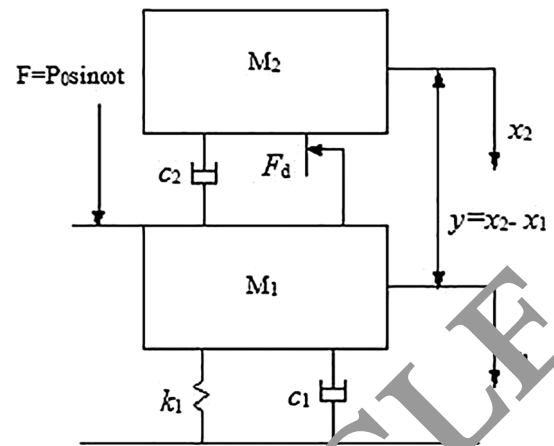


Fig. 1 Kinetic model of boring bar

$M_1$  and  $K_1$  are mass of the main structure and elasticity coefficient, respectively.  $m_2$  is mass of the additional structure. There are damping  $c_2$  and friction  $F_d$  between  $M_1$  and  $M_2$ .  $\omega$  is excitation frequency.  $P_0$  is amplitude of excitation force. For solving and measuring the system, it needs excitation to make the system vibrate. There are three kinds of excitation: steady-state sinusoidal excitation, random excitation and transient excitation. Therefore, we use the most common steady-state sinusoidal excitation which also known as simple harmonic excitation; its advantages are large excitation power, high signal–noise ratio and high test precision.

Friction is the important part of boring bar we researched, and we choose the dry friction model that the sliding friction coefficient is characterized as polynomial function of relative velocity. And this model has been successfully used to analyze friction natural vibration [8, 9]. Changing curve of sliding friction coefficient  $\mu_d$  and changing curve of dry friction force  $F_d$  with velocity are shown in Figs. 2 and 3, respectively. According to figures, the time when relative velocity  $|\dot{y}| < v_m$ ,  $\mu_d$  increases with decreasing of  $|\dot{y}|$  and when relative  $|\dot{y}| > v_m$ ,  $\mu_d$  increases with increasing of  $|\dot{y}|$  are shown. And the time when  $|\dot{y}| = v_m$ ,  $\mu_d$  reaches the minimum. Dry friction force can be approximately expressed as follow equation.

$$F_d = F_f \operatorname{sgn}(\dot{y}) - B_1 \dot{y} + B_2 \dot{y}^3 = \mu_d F \quad (1)$$

In the equation,  $F_f > 0$ ,  $B_1 > 0$ ,  $B_2 > 0$ , and they are constant.  $\mu_d$  is the friction coefficient.  $F$  is the positive pressure.

Establish differential equations for  $M_1$  and  $M_2$  as follows.

$$m_2 \ddot{x}_2 + c_2 \dot{y} + F_d(\dot{y}) = 0 \quad (2)$$

$$m_1 \ddot{x}_1 + c_1 \dot{x}_1 + k_1 x_1 - c_2 \dot{y} - F_d(\dot{y}) = P_0 \sin \omega t \quad (3)$$

wherein  $m_1$ ,  $c_1$  and  $k_1$  are modal mass coefficient, modal damping coefficient and modal stiffness coefficient of

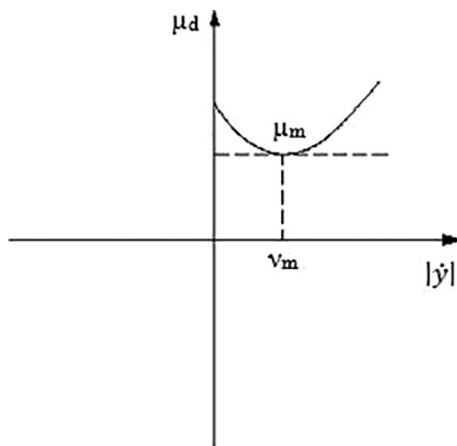


Fig. 2 Changing curve of sliding friction coefficient

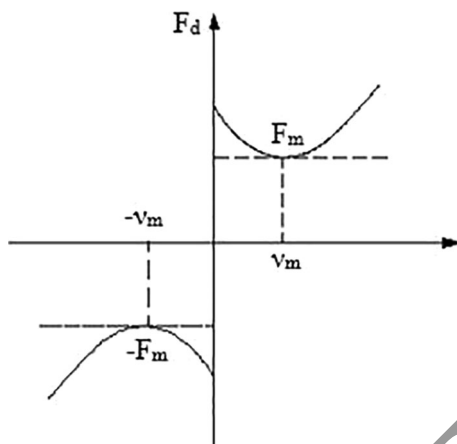


Fig. 3 Changing curve of dry friction

boring bar, respectively.  $m_2$ ,  $c_2$  and  $k_2$  are modal mass coefficient, modal damping coefficient and modal stiffness coefficient of built-in subsystem 2, and  $\omega$  are the amplitude and frequency of sine excitation, respectively.

During the cutting process, the vibration of the boring bar is not very big, and the corresponding value is only several millimeter. As a result,  $x$  and  $y$  are also small. Finally, in the above equations, high-order harmonics in the solution will be very small when it is compared with the low-order harmonics. So the high-order harmonics can be neglected, and the corresponding solution is shown in the following.

$$x_1 = x_m \sin(\omega t - \phi_x) \quad y = y_m \sin(\omega t - \phi_y) \quad (4)$$

Figure 4 only shows waveform of the first term  $F_f \text{sgn}(\dot{y})$  in Eq. (1). According to the published paper [1],  $\text{sgn}(\dot{y})$  is a sign function in which period is  $3\pi/2$ , and waveform of the sign function is a square wave as shown in Fig. 4. This detailed type of the sign function can be determined by experiments (Fig. 5).

Make Fourier series expansion for  $\tilde{F}(\omega\tau)$  as follows.

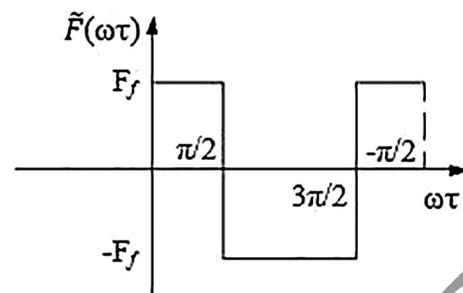


Fig. 4 Square wave of friction force

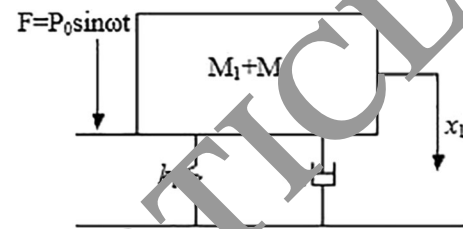


Fig. 5 Model in bonding state

$$\tilde{F}(\omega\tau) = \frac{F_f}{2} \sum_{n=1}^{\infty} a_n \cos n\omega\tau + b_n \sin n\omega\tau \quad (5)$$

According to Fig. 4, Eq. (5) is a period function,  $a_0 = 0$ , and  $a_n = b_n$ .

$$a_n = b_n = \begin{cases} \frac{4F_f}{n\pi} \left[ \sin \frac{n\pi}{2} \right], & n = 2m + 1 \\ 0, & n = 2m + 2 \end{cases} \quad m = 0, 1, 2, \dots \quad (6)$$

As a square wave of ideal dry friction model which is well-known as Coulomb dry friction, the approximate solution can take the first term of its Fourier series [10], and the approximation is consistent with the exact solution well [11]. So take the first term of series expansion instead and contact Eq. (4), approximate solution can be obtained as follows.

$$\tilde{F}(\omega t) \approx \frac{4F_f}{\pi} \cos(\omega t - \theta) \quad (7)$$

With Eq. (1), the equation can be expressed as follows.

$$F_d(\dot{y}) = \frac{4F_f}{\pi} \cos(\omega t - \theta) - B_1 \dot{y} + B_2 \dot{y}^3 \quad (8)$$

### 3 Initial simulation results based on MATLAB

As known from the above model, the vibration reduction effect generated by the friction damper with the dry friction changing can be researched when the other parameters are not changed. Wherein,  $M_1 = 2.9$  kg,  $M_2 = 1.1$  kg,  $c_1 = 0.076$ , and  $k_1 = 2,500,000$  N/m. The above formula

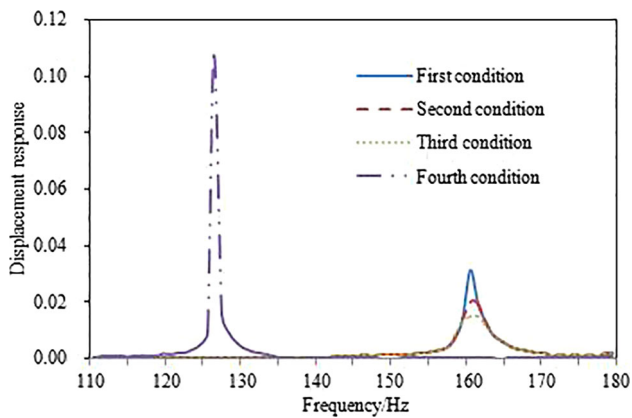


**Fig. 6** Displacement frequency response of the boring system

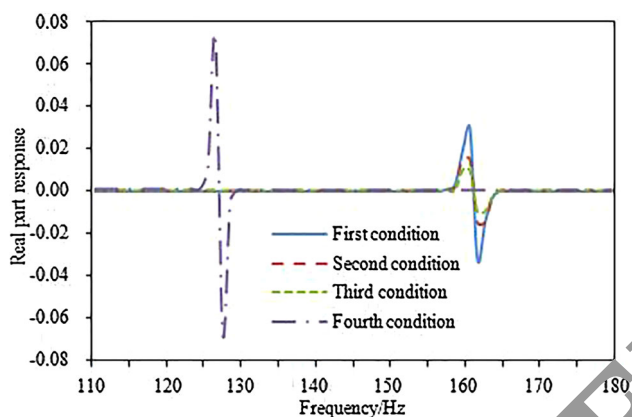
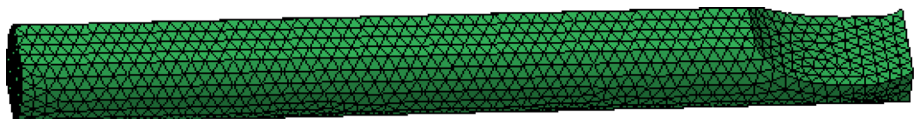


**Fig. 7** Changing curve of real part frequency response

is programmed by MATLAB, so as to obtain the displacement frequency response and real part changing curve of the boring bar, as shown in Figs. 6 and 7.

The fourth curve is the displacement frequency response curve without friction. Meanwhile, the vibrator and the main system are in the adhered state. As can be seen from the above figures, the friction damper which is in the adhered state is equivalent to a system with single degree of freedom. And the natural frequency of the boring bar is reduced, the amplitude is increased, the largest real part is also enlarged, and the vibration reduction effect of the boring bar is greatly reduced. However, the friction damper has an effect on the remaining curves. Among them, the friction damping of the first curve is small, and the second one is moderate, while the third one is large. As known from the above

**Fig. 8** Finite element model of the boring bar



simulation result, the response magnitude of the boring bar is decreased with the increase in the friction damping, and the friction plays an important effect on the vibration reduction. There are two obvious peaks in Fig. 7 because they are from the structural resonance.

#### 4 Finite element model verification and reality of the virtual boring bar

From the above analysis, the friction plays an important role in the vibration reduction process of the boring bar. However, more perfect results cannot be obtained only through MATLAB software, because the computation based on the theory has been simplified to some extent, and the virtual boring bar cannot be realized. As a result, it cannot reflect the actual situation exactly. Therefore, it is necessary to build the finite element model to conduct the simulation analysis and reality of the virtual. The boring bar is divided into a lot of tetrahedral meshes, and constraints are implied on its internal structure. The end of the boring bar is fixed, while the other end is free to cut the work piece. As a result, the finite element model of the boring bar can be obtained as shown in Fig. 8. It has 10,296 elements and 11,269 nodes, and the computational software is ABAQUS. Then, the finite element mesh is given the material properties, in order to solve the first 6-order modes, as shown in Fig. 9. In Fig. 9, there are some bending and twisting modes. The fixed end is not changed. The serious vibration is in the free end of the boring bar, and it is also the work end.

As the internal structure of the boring bar is very complex, it is necessary to verify the finite element model by experiments, whose results are shown in Table 1. It is indicated that the relative errors between the experimental and simulation values of the boring bar are controlled within 5% which is allowable error in engineering. Therefore, the finite element model in this paper is reliable.

#### 5 Experiment and simulation of the cutting process for the boring bar

In order to verify the applicability of the boring bar, the actual cutting experiment is conducted, with acceleration sensor arranged in the boring bar. In the platform of the experiment, LabVIEW is applied to make a set of signal

**Fig. 9** First 6-order modes of the boring bar



acquisition program, and the acquisition of vibration signals is realized on PXI-1042Q data acquisition computer. The experimental data can be exported from the acquisition system, and MATLAB program is used to analyze the cutting vibration data.

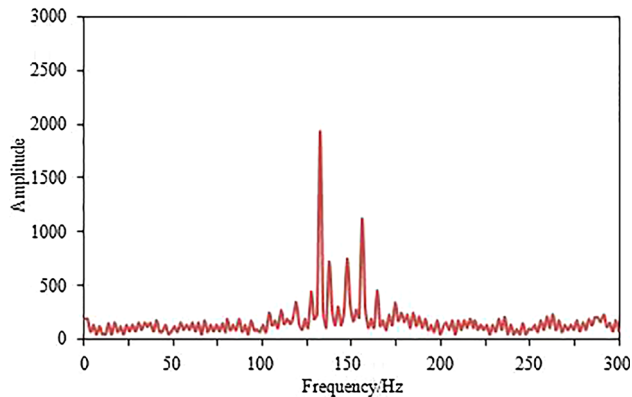
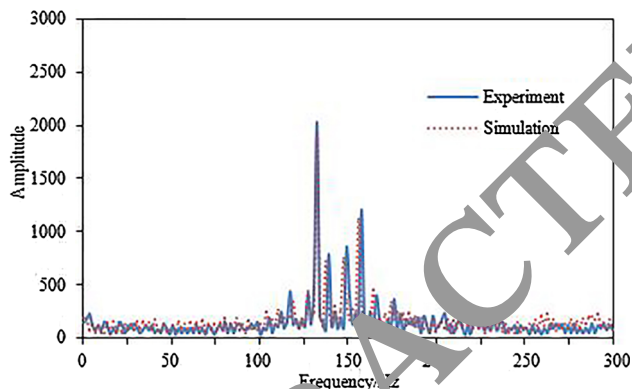
The experimental conditions are given. The overhang length of the boring bar is 450 mm, boring bar diameter is 40 mm, rotation speed is 500 rpm, back cutting depth is 0.2 mm, feed rate is 0.18 mm/r, cutting speed is 70 m/min,

and positive pressure between the friction vibrator and boring bar is 5 N. Finally, the frequency response curve of the boring bar is obtained, as shown in Fig. 10. It can be seen that the energy of the frequency response curve is basically concentrated in the 100–200 Hz.

According to the experimental conditions and the finite element model of the boring bar, the cutting process simulation model of the boring bar is built and the frequency response curve is then computed, which is compared with

**Table 1** Comparison of the experimental and simulation values regarding first 6-order modes

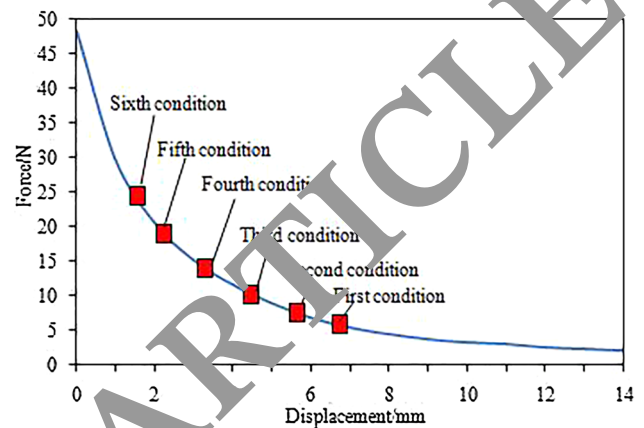
Order	Simulation value/Hz	Experimental value/Hz	Relative error/%
1	7.42	7.69	-3.50
2	45.76	44.12	3.71
3	125.56	122.36	2.61
4	238.24	241.25	-1.25
5	278.66	270.69	2.94
6	374.73	380.05	-1.40

**Fig. 10** Cutting frequency response curve of the boring bar**Fig. 11** Comparison of the cutting frequency response curve between simulation and experiment

the experimental value in Figs. 10 and 11. It can be seen that the difference between simulation and experimental results is very small. Therefore, it indicates the cutting simulation model is reliable and can be used to conduct the subsequent analysis.

## 6 Parameter analysis of cutting process for the boring bar

The boring bar vibration in the cutting process is affected by many factors, such as positive pressure between the friction vibrator and boring bar, cutting speed, feed rate and

**Fig. 12** Positive pressure between the friction vibrator and boring bar

back cutting depth. The size of the cutting force is directly affected by these factors. As a result, the dynamic characteristics of the boring bar will be also affected by these factors. Therefore, it is necessary to analyze and research these factors, so as to obtain a boring bar with better vibration reduction performance.

### 6.1 Positive pressure between the friction vibrator and boring bar

The cutting speed is 70 m/min, feed rate is 0.18 mm/r, and back cutting depth is 0.2 mm, while the positive pressure between the friction vibrator and boring bar is changed as shown in Fig. 12. Through the verified simulation model, the frequency response of the boring bar under different pressures is computed as shown in Fig. 13. It can be seen from the figure that the amplitude of the spectrum firstly decreases and then increases with the increasing positive pressure. The third condition has the minimum frequency response amplitude, and the energy distribution of each frequency is evenly instead of concentrated in a band, so the vibration reduction effect is better. Under the sixth condition, the positive pressure between the friction vibrator and boring bar is greater, which prevents them from the relative sliding. Therefore, the vibration reduction effect is not obvious, and the frequency response is large.

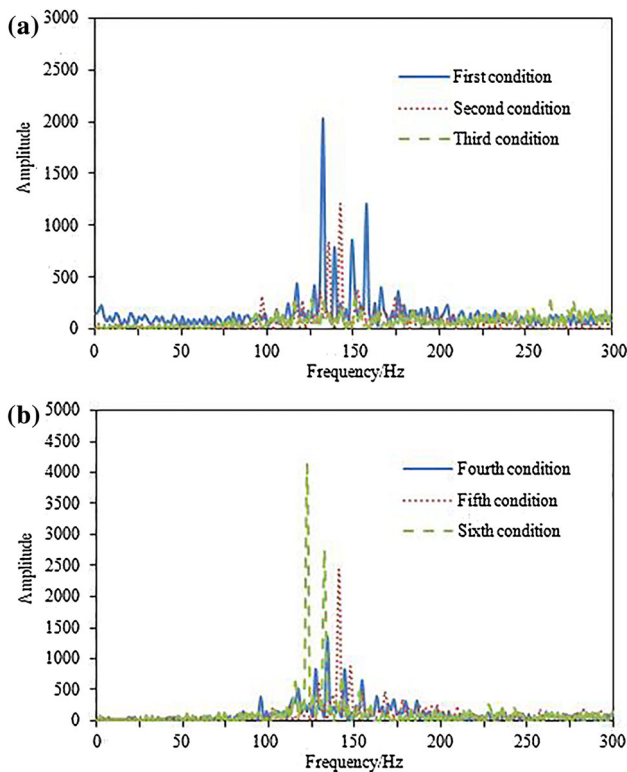


**Fig. 13** Frequency response curve of the boring bar under different pressures. **a** Frequency response of the boring bar under the first three pressures, **b** frequency response of the boring bar under the last three pressures

### 6.2 Cutting speed

The positive pressure is 10 N, feed rate is 0.18 mm/r, and back cutting depth is 0.2 mm, while the cutting speed is changed from 70 to 90 m/min with the step size of 10 m/min. The frequency response curve of the boring bar under different cutting speeds is obtained as shown in Fig. 14. As can be seen from the figure, the frequency response amplitude of the boring bar is decreased gradually along with the increase in cutting speed. Thus, the greater value regarding the cutting speed of the boring bar should be preferred in the actual cutting engineering.

### 6.3 Feed rate

The positive pressure is 10 N, cutting speed is 90 m/min, and back cutting depth is 0.2 mm, while the feed rate is changed from 0.18 to 0.38 mm/r with the step size of 0.1 mm/r. The frequency response curve of the boring bar under different feed rates is obtained as shown in Fig. 15. As can be seen from the figure, the frequency response amplitude of the boring bar is gradually increased along with the increase in feed rate. Thus, the

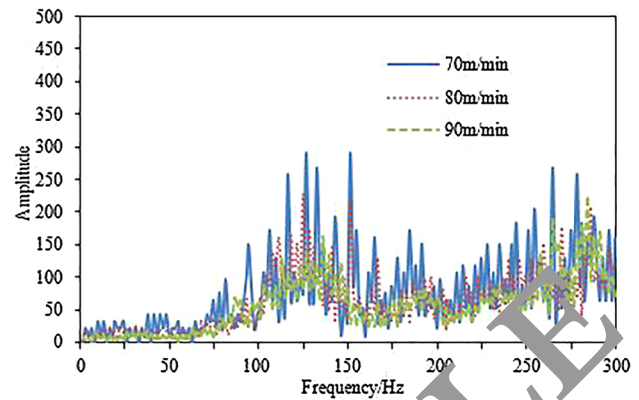


**Fig. 14** Frequency response curve of the boring bar under different cutting speeds

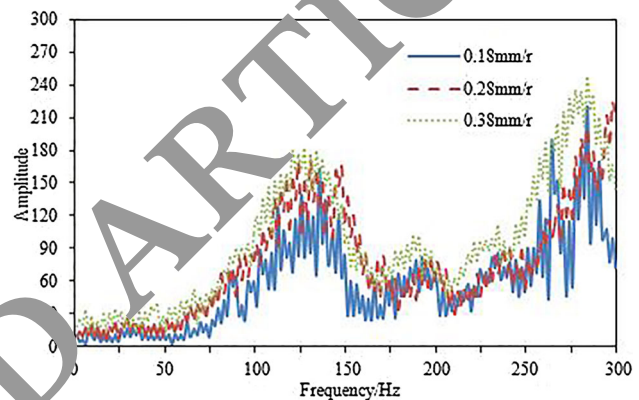


**Fig. 15** Frequency response curve of the boring bar under different feed rates

smaller feed rate should be chosen in the cutting process of the boring bar.

### 6.4 Back cutting depth

The positive pressure is 10 N, cutting speed is 90 m/min, and feed rate is 0.18 mm/r, while the back cutting depth is changed from 0.2 to 0.4 mm with the step size of 0.1 mm. The frequency response curve of the boring bar under different back cutting depths is obtained as shown in Fig. 16. As can be seen from the figure, the frequency response amplitude of the boring bar is gradually increased along with the increase in back cutting depth. Thus, the smaller back cutting depth should be chosen in the cutting process of the boring bar.

## 7 Optimization of the cutting process based on PSO-BP neural networks

Finite element software is usually used for response analysis when direct computation is applied to conduct structural optimization in actual engineering. With the

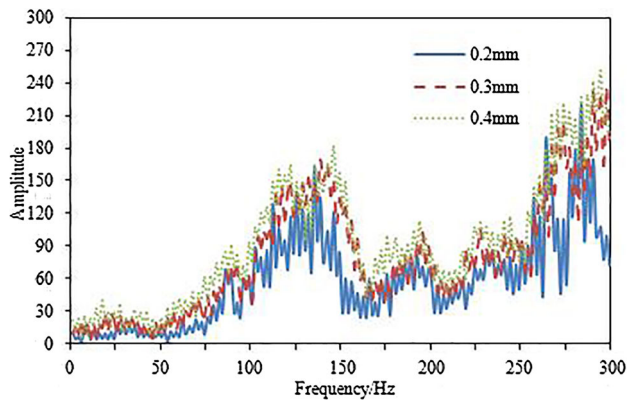


**Fig. 16** Frequency response curve of the boring bar under different back cutting depths

increasing complexity of optimized structures, finite element models have been larger and more refined and the response analysis of finite element software has spent more time, which reduces optimization efficiency. Aimed at this situation, models of fast operation are introduced into the field of the structural engineering. At present, response surface and neural network are representative models. Neural network is a mathematical model which is designed by simulating the information processing of human nervous system. With strong function approximation ability and impressive performance in parallel computing, neural network is more and more widely applied in the computation and simulation of structures. Numerous studies show that neural network with a hidden layer can approximate to any continuous functions. To optimize the cutting process and precision of the boring bar, this paper adopts a BP neural network structure with a hidden layer [10–12], as shown in Fig. 17. To improve precision, the number of neurons in the hidden layer is set as 13, and training is conducted for BP neural network. The computational software of the neural network is MATLAB in this paper. Training error is shown in Fig. 18. It can be seen from Fig. 18 that the output result of neural network is basically stable when the number of iterations of training is 800. This process takes a lot of time, and optimization efficiency is low.

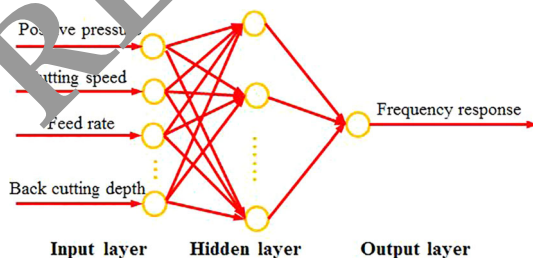


**Fig. 17** Topology result of BP neural network of the optimized boring bar

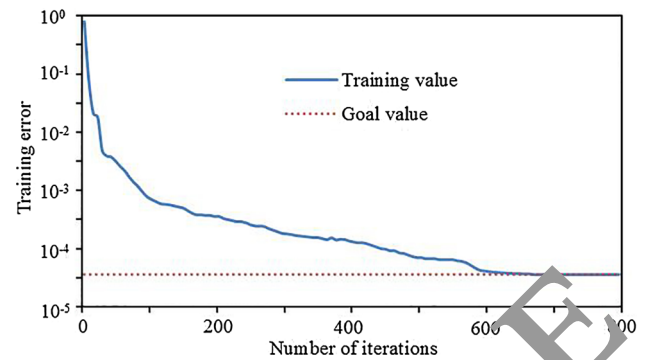


**Fig. 18** Training error of BP neural network

As a widely common network model, BP neural network has clear and understandable principle, rigorous process and strong universality. However, it can be found from the above analysis that BP neural network also has some deficiencies like slow convergence speed and long training time. When training is carried out to a certain extent, situations like the drop of error and the sharp decline of rate usually take place, which is caused by the small learning rate and slow learning speed set by standard BP algorithm in order to guarantee system stability. Apart from the drop of error and the decline of rate, the drop and stagnation of error also appear in the process of training, which results in local minimum. As BP algorithm adopts gradient descent method, training process drops to the minimum along the bevel face of error function. Aimed at the deficiencies of BP neural networks, a structural model of BP neural network based on particle swarm optimization [13–16] is proposed to solve the problem of falling into local extremum easily.

PSO algorithm is based on global search, whose optimization starts from multiple random particles and searches the space around these particles. Compared with BP algorithm, PSO algorithm optimizes multiple random points, with fast convergence speed. In addition, updating the location and speed of each particle will be affected by other particles. Then, a particle is very likely to jump out of local extremum under the influence of other particles after falling into local extremum. By contrast, BP algorithm only has one particle which will find it difficult to jump out of local extremum once it falls into it. As a result, the introduction of PSO algorithm into BP neural network will possibly solve the problems of BP network including slow convergence speed and falling into local extremum easily. PSO algorithm does not directly optimize the objective function, but conducts optimization according to the fitness function corresponding to the objective function. Independent of the gradient information of error function, PSO algorithm will have a wider range of application. The process of PSO-BP neural network algorithm [17–25] is shown in Fig. 19.



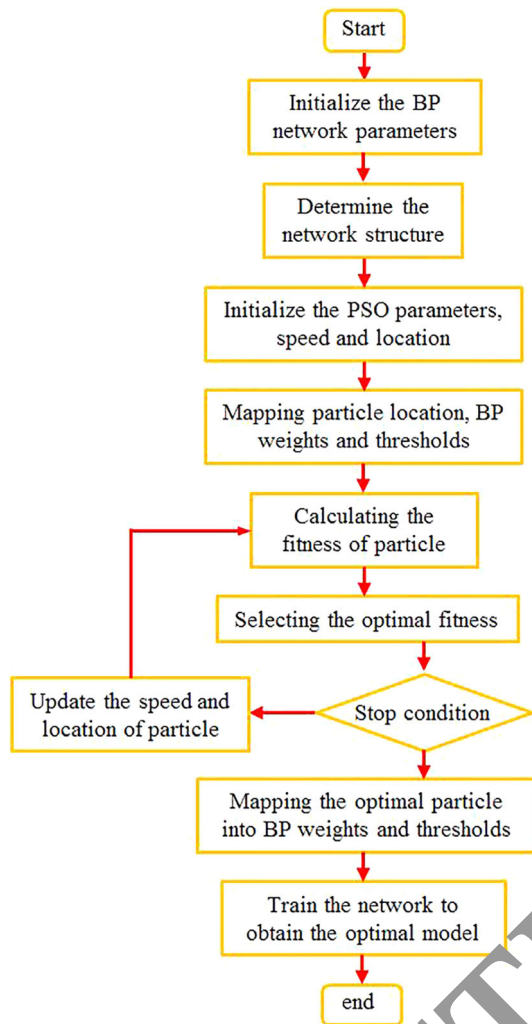


Fig. 19 Flow chart of PSO-BP neural network

The first step is to initialize BP neural network, mainly including setting the number of neurons in the input layer and output layer [26–28], and number of layers and neurons in the hidden layer, and parameters like learning rate and error value.

The second step is to initialize the particle swarm, mainly including setting the number of particles, initial position, initial velocity, maximum speed and so on.

The third step is to compute fitness value and initialize global optimal point and individual optimal point, including putting initialized particles into BP neural network, computing the mean square error of training output and sample output of neural network according to fitness function and initializing global optimum and individual optimum.

The fourth step is to update the extremum. Compared with the individual value of particles, the current optimum will be given to individual particles if the current optimum is more optimal.

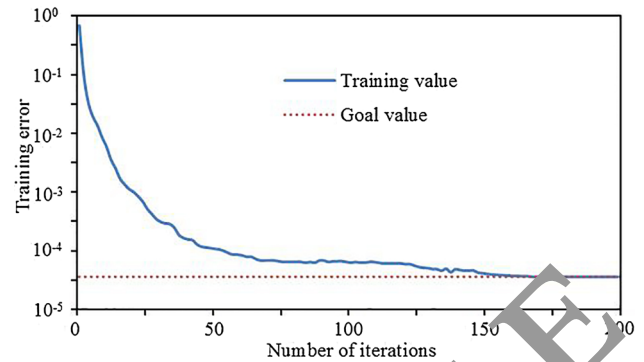


Fig. 20 Training error of PSO-BP neural network

The fifth step is to update the speed and location, including adjusting the speed of each particle according to the formula of speed update and adjusting the location of each particle according to location.

The sixth step is to check whether the conditions of stopping iteration are met. If globally optimal solution is less than the specified error or the number of iterations is maximum, and iteration will be stopped and weights and thresholds of neural network will be outputted. Otherwise, it will switch to the third step.

The improved BP neural network is used to optimize the cutting process of the boring bar. Firstly, training is carried out for neural network. Training error is shown in Fig. 20. It can be seen from Fig. 20 that PSO-BP neural network tends to be stable when the number of iterations is 200. Compared with original BP neural network, optimization efficiency is obviously improved. Based on the above optimization algorithm, the optimal parameter in the cutting process of the boring bore can be obtained. It can be determined that when the positive pressure between the friction vibrator and boring bar is 10 N, cutting speed is 90 m/min, feed rate is 0.18 mm/r, and back cutting depth is 0.2 mm, the boring bar has better vibration reduction effect. In order to verify the optimized effect, the parameters of the cutting experiment are set according to the above experiment so as to cut the work piece. And its result is compared with the result of the original cutting parameters, as shown in Fig. 21. It can be seen that the cutting quality has significantly improved after optimizing the boring bar. Therefore, it is indicated that the optimized boring bar in this paper is effective. Therefore, we can obtain higher quality work piece when we use this boring bar in the actual engineering.



Fig. 21 Experimental verification of the cutting precision

## 8 Conclusions

1. Based on the traditional boring bar, a boring bar with friction damper is proposed in the paper. Then, the frequency response under different pressures is computed primarily based on the theory, which shows that the proposed boring bar has a certain vibration reduction effect.
2. The finite element model of the boring bar is built, and the first 6-order modes are computed, whose results are compared with the experimental value. They are consistent with each other, which show that the finite element model is reliable. The experimental cutting process of the boring bar is researched, which is compared with the simulation model with good coincidence. It is found from the result that the cutting simulation model of the boring bar is effective.
3. Based on the verified simulation model, the positive pressure between the friction vibrator and boring bar, cutting speed, feed rate, back cutting depth and other parameters are changed to study the vibration reduction effects of the boring bar with friction damper. PSO-BP neural network is then used to optimize the cutting process of the boring bar, and the optimal cutting parameters can be obtained. Finally, these optimized parameters are applied in the boring bar, the vibration reduction effect of the boring bar is verified by means of experiments, and the corresponding result shows that the proposed optimization in this paper is feasible. We can obtain higher quality work piece when we use this boring bar in the actual engineering. In the future work, we want to change the internal structure of the boring bar to improve the cutting result.

### Compliance with ethical standards

**Conflict of interest** We declare that this manuscript has no any conflict of interest and has not submitted and published in the other journal, and it was only submitted to Neural Computing and Applications.

## References

1. Mei J, Kong T, Shih AJ et al (2009) Magnetorheological fluid-controlled boring bar for chatter suppression. *J Mater Process Technol* 209(4):1861–1870
2. Moradi H, Bakhtiari-Nejad F, Movahhedy MR (2008) Tuneable vibration absorber design to suppress vibrations: an application in boring manufacturing process. *J Sound Vib* 318(1):93–108
3. Miguelez MH, Rubio L, Loya JA et al (2010) Improvement of chatter stability in boring operations with passive vibration absorbers. *Int J Mech Sci* 52(10):1376–1384
4. Sims ND (2007) Vibration absorbers for chatter suppression: a new analytical tuning methodology. *J Sound Vib* 301(3):592–607
5. Yao Z, Chen Z, Mei D (2011) Chatter suppression by parametric excitation: model and experiments. *J Sound Vib* 330(13):2995–3005
6. Andr n L, H kansson L, Brandt A et al (2004) Identification of motion of cutting tool vibration in a continuous boring operation—correlation to structural properties. *Mech Syst Signal Process* 18(4):903–927
7. Zhai P, Zhang CR, Liu SY, Wang HT (2006) Dynamic design of a high frequency response servo bar used for boring. *Manuf Technol Mach Tool* 8:103–106
8. Mei D, Yao Z, Kong T et al (2010) Parameter optimization of time-varying stiffness method for chatter suppression based on magnetorheological fluid-controlled boring bar. *Int J Adv Manuf Technol* 46(9–12):1071–1083
9. Al-Wedyan HM, Bhat RB, Demirli K (2007) Whirling vibrations in boring trepanning association deep hole boring process: analytical and experimental investigations. *J Manuf Sci Eng* 129(1):48–62
10. Yi J, Wang Q, Zhao D et al (2007) A neural network prediction-based variable-period sampling approach for networked control systems. *Appl Math Comput* 183(2):976–988
11. Zhang JH, Xie AG, Shen JM (2007) Multi-objective optimization and analysis model of shaper process based on BP neural network. *J Iron Steel Res Int* 14(2):1–5
12. Assarzadeh S, Gholaei M (2008) Neural-network-based modeling and optimization of the electro-discharge machining process. *Int J Adv Manuf Technol* 39(5–6):488–500
13. Park J, Lee KS, Shin JR et al (2005) A particle swarm optimization for economic dispatch with nonsmooth cost functions. *IEEE Trans Power Syst* 20(1):34–42
14. Del Valle Y, Venayagamoorthy GK, Mohagheghi S et al (2008) Particle swarm optimization: basic concepts, variants and applications in power systems. *IEEE Trans Evol Comput* 12(2):171–195
15. Jiang M, Luo YP, Yang SY (2007) Stochastic convergence analysis and parameter selection of the standard particle swarm optimization algorithm. *Inf Process Lett* 102(1):8–16
16. Chatterjee A, Siarry P (2006) Nonlinear inertia weight variation for dynamic adaptation in particle swarm optimization. *Comput Oper Res* 33(3):859–871
17. Khan K, Sahai A (2012) A comparison of BA, GA, PSO, BP and LM for training feed forward neural networks in e-learning context. *Int J Intell Syst Appl* 4(7):23
18. Ping W, Huang Z, Zhang M et al (2008) Mechanical property prediction of strip model based on PSO-BP neural network. *J Iron Steel Res Int* 15(3):87–91
19. Taormina R et al (2015) Data-driven input variable selection for rainfall-runoff modeling using binary-coded particle swarm optimization and Extreme Learning Machines. *J Hydrol* 529(3):1617–1632
20. Zhang J et al (2009) Multilayer ensemble pruning via novel multi-sub-swarm particle swarm optimization. *J Univers Comput Sci* 15(4):840–858
21. Wang WC et al (2015) Improving forecasting accuracy of annual runoff time series using ARIMA based on EEMD decomposition. *Water Resour Manag* 29(8):2655–2675
22. Zhang SW et al (2009) Dimension reduction using semi-supervised locally linear embedding for plant leaf classification. *Lect Notes Comput Sci* 5754:948–955
23. Wu CL et al (2009) Methods to improve neural network performance in daily flows prediction. *J Hydrol* 372(1–4):80–93
24. Chau KW et al (2010) A hybrid model coupled with singular spectrum analysis for daily rainfall prediction. *J Hydroinform* 12(4):458–473
25. Illias HA, Chai XR, Mokhlis H (2015) Transformer incipient fault prediction using combined artificial neural network and

- various particle swarm optimisation techniques. PLoS ONE 10(6):e0129363
26. Lv Z, Tek A, Da Silva F et al (2013) Game on, science-how video game technology may help biologists tackle visualization challenges. PLoS ONE 8(3):e57990
  27. Wei W, Xu Q, Wang L et al (2014) GI/Geom/1 queue based on communication model for mesh networks. Int J Commun Syst 27(11):3013–3029
  28. Lv Z, Chen G, Zhong C et al (2012) A framework for multi-dimensional webgis based interactive online virtual community. Adv Sci Lett 7(1):215–219

RETRACTED ARTICLE